Molecular Cell
Article

The Molecular Basis of ABA-Independent Inhibition of PP2Cs by a Subclass of PYL Proteins

Qi Hao,[1,2,6] Ping Yin,[1,2,6] Wenqi Li,[1,2,6] Li Wang,[3,7] Chuangye Yan,[1,2,7] Zhaohu Lin,[4] Jim Zhen Wu,[4] Jiawei Wang,[1,2] S. Frank Yan,[5] and Nieng Yan[1,2,*]
[1]State Key Laboratory of Biomembrane and Membrane Biotechnology
[2]Center for Structural Biology, School of Medicine and School of Life Sciences
Tsinghua University, Beijing 100084, China
[3]School of Life Sciences, Peking University, Beijing 100080, China
[4]Discovery Biology
[5]Molecular Design and Biostructure
Roche Pharma Research and Early Development China, 720 Cai Lun Road, Building 5, Shanghai 201203, China
[6]These authors contributed equally to this work
[7]These authors contributed equally to this work
*Correspondence: nyan@tsinghua.edu.cn
DOI 10.1016/j.molcel.2011.05.011

SUMMARY

PYR1/PYL/RCAR proteins (PYLs) are confirmed abscisic acid (ABA) receptors, which inhibit protein phosphatase 2C (PP2C) upon binding to ABA. *Arabidopsis thaliana* has 14 PYLs, yet their functional distinction remains unclear. Here, we report systematic biochemical characterization of PYLs. A subclass of PYLs, represented by PYL10, inhibited PP2C in the absence of any ligand. Crystal structures of PYL10, both in the free form and in the HAB1 (PP2C)-bound state, revealed the structural basis for its constitutive activity. Structural-guided biochemical analyses revealed that ABA-independent inhibition of PP2C requires the PYLs to exist in a monomeric state. In addition, the residues guarding the entrance to the ligand-binding pocket of these PYLs should be bulky and hydrophobic. Based on these principles, we were able to generate monomeric PYL2 variants that gained constitutive inhibitory effect on PP2Cs. These findings provide an important framework for understanding the complex regulation of ABA signaling by PYL proteins.

INTRODUCTION

Abscisic acid (ABA) is an essential phytohormone that protects plants against biotic and abiotic stress (Fedoroff, 2002; Finkelstein et al., 2008; Schroeder and Nambara, 2006; Zhu, 2002). Members of the PYR1/PYL/RCAR family of proteins (hereafter referred to as PYLs for simplicity) are ABA receptors in the cytoplasm and nucleus (Ma et al., 2009; Park et al., 2009; Santiago et al., 2009b). PYLs, comprised of 14 members (PYR1 and PYL1-13) in *Arabidopsis thaliana*, belong to plant pathogenesis-related proteins of class 10 (PR-10) (van Loon et al., 2006), each containing a characteristic START (star-related lipid transfer) domain (Iyer et al., 2001). Biochemical and structural investigations revealed the molecular mechanisms by which PYLs inhibit some members of group A protein phosphatases type 2Cs (PP2Cs), such as ABI1 and HAB1, in an ABA-dependent manner (Melcher et al., 2009; Miyazono et al., 2009; Nishimura et al., 2009; Santiago et al., 2009a; Yin et al., 2009).

ABA is accommodated by a conserved, water-filled pocket in PYLs. The ligand-binding pocket is surrounded by four highly conserved surface loops, which we named CL1 through CL4 (Yin et al., 2009). Upon ABA binding, the switch loop CL2 undergoes pronounced conformational rearrangement and creates a surface for interaction with PP2Cs (Melcher et al., 2009; Nishimura et al., 2009; Santiago et al., 2009a; Yin et al., 2009). Formation of the ABA-PYL-PP2C complex blocks substrate entry to PP2C, relieving PP2C-mediated inhibition of the downstream SnRK2 kinases (Melcher et al., 2009; Miyazono et al., 2009; Yin et al., 2009). SnRK2 kinases, activated upon autophosphorylation, phosphorylate and activate the transcription factors that induce the expression of ABA-responsive genes. This linear pathway has been elegantly recapitulated in vitro (Fujii et al., 2009).

Despite recent breakthrough in the elucidation of PYLs-mediated ABA signaling (Cutler et al., 2010; Hubbard et al., 2010; Klingler et al., 2010; Melcher et al., 2010b), a number of questions remain unanswered. In particular, there are 13 ABA-responsive PYLs, which share a high degree of sequence identity, especially for the residues that are involved in ligand recognition and PP2C interaction (Yin et al., 2009). It is unclear whether they are functionally distinct in ABA signaling. Notably, preliminary in vivo and in vitro characterization suggested that some PYL proteins may bind to and inhibit PP2Cs even in the absence of ABA (Fujii et al., 2009; Nishimura et al., 2010; Park et al., 2009), although the molecular mechanism remains elusive. In addition, the published structures of PYR1, PYL1 and PYL2 revealed a dimeric arrangement for both ligand-free and ABA-bound PYLs. But the ABA-bound PYL forms a 1:1 complex with PP2C. It was suggested that ABA binding weakened the dimer formation of PYL2 (Yin et al., 2009). What is the functional role of dimer formation for PYLs? Are there monomeric PYLs? If so, are there functional consequences that distinguish monomer and dimer?

To address these important questions, we launched a systematic biochemical characterization of PYL proteins. Except for PYLs 7, 11, 12, and 13, which defied recombinant expression or purification, all PYL proteins from *Arabidopsis thaliana* were expressed and purified to homogeneity. We examined their ability to inhibit the phosphatase activity of four PP2Cs, including ABI1, HAB1, HAB2, and PP2CA, in the presence or absence of ABA. Interestingly, a subclass of PYL proteins, exemplified by PYL10, exhibited constitutive binding and inhibition of PP2Cs even in the absence of any ligand. By contrast, PYR1 and PYLs 1–3 relied on ABA for the inhibition of PP2Cs.

We focused on PYL10 for detailed structural and biochemical analyses, which suggested principles for the constitutive inhibition of PP2Cs by PYL10. On the basis of these principles, we were able to engineer variants of PYL2 that gained the constitutive activity. The results reported here provide important insights into the delineation of the seemingly redundant PYL proteins and shed light on the potential engineering of transgenic plants that may exhibit enhanced tolerance to environmental stress.

RESULTS

A Subclass of PYLs Exhibits Constitutive Inhibition of PP2Cs

We examined the inhibitory effects of ten PYLs on the phosphatase activity of ABI1, HAB1, HAB2, and PP2CA. The phosphatase activity was measured by the Ser/Thr phosphatase assay system (Promega) according to published protocols (Yin et al., 2009). In the presence of 10 μM (+)-ABA (hereafter referred to ABA), most of the PYL proteins, each at 4 μM concentration, could completely inhibit the phosphatase activity of approximately 0.4 μM PP2Cs (Figure S1, left panels, available online). The only exception was PYL6, which inhibited about 80% of the phosphatase activity of PP2CA. Unexpectedly, in the control experiment, PYLs 5–10 (except the untested PYL7) appeared to inhibit some PP2Cs to certain degrees even in the absence of any ligand.

Next, we carefully examined the inhibitory effect on the four PP2Cs by PYLs in the absence of ligand, with the PYL:PP2C ratios of 1:1, 10:1, and 100:1. Upon addition of certain PYLs, the phosphatase activities of the PP2Cs were enhanced considerably (Figure S1, right panels). Reasoning that it might be caused by protein crowding, we tested the effect of bovine serum albumin (BSA) and a loss-of-function mutant PYL2-S2R (S89R, S94R) (Yin et al., 2009). Indeed, addition of BSA or PYL2-S2R to the tested PP2Cs both led to increased phosphatase activity, particularly for HAB1 (Figure S1, right panels). Therefore, we normalized all the assay data with the phosphatase activities in the presence of PYL2-S2R at three corresponding concentrations as 100% and the ones without phosphatase as zero (Figure 1).

PYR1 and PYLs 1–3 failed to exhibit prominent inhibition of ABI1, HAB2, and PP2CA (Figure 1), but they all showed weak inhibitory effects on HAB1 when added in 100-fold excess (Figure 1B). PYL10, on the other hand, appeared to be a potent "constitutive inhibitor." It was able to inhibit up to 80% of the phosphatase activity of ABI1 at a PYL:PP2C ratio of 1:1 and abrogated the phosphatase activity of ABI1 when added in 10-fold molar excess (Figure 1A). This observation is consistent with the previous report that ABA-responsive gene expression could be induced when ABF2, SnRK2.6, ABI1, and PYL10 were coexpressed in *Arabidopsis* protoplasts even without ABA treatment (Fujii et al., 2009). PYL10 also displayed significant inhibition of HAB1 and HAB2 at a PYL:PP2C molar ratio of 10:1 and completely inhibited these two PP2Cs at a ratio of 100:1 (Figures 1B and 1C). The inhibitory effect on PP2CA appeared to be weaker. PYL10 inhibited approximately 50% and 80% of the phosphatase activity of PP2CA at protein ratios of 10:1 and 100:1, but showed no inhibition at the ratio of 1:1 (Figure 1D).

Other than PYL10, PYLs 5–9 (except the untested PYL7) also inhibited the four PP2Cs to various degrees in the absence of ligand. PYL4, on the other hand, only showed clear inhibition of HAB2 (Figure 1C), but not the other three PP2Cs. Therefore, the in vitro activity assay identified a subclass of PYLs that showed constitutive inhibition of the phosphatase activity of PP2Cs even in the absence of ABA.

PYL10 Forms Stable Complexes with PP2Cs in the Absence of ABA

To understand the molecular basis underlying the constitutive inhibition of PP2Cs by PYLs, we focused on PYL10 for further biochemical and structural investigations. First, we examined whether PYL10 and PP2C could form a stable complex in the absence of ABA. PYL10 and PP2Cs were each purified to homogeneity, and their interactions were assessed by size-exclusion chromatography (SEC). PYL2, whose interaction with ABI1 strictly relies on ABA (Park et al., 2009; Yin et al., 2009), was included as control (Figure 2A, upper panels). The elution volumes of PYL10 and ABI1, in their free form, were approximately 16.2 ml and 15.8 ml, respectively. Upon coincubation, PYL10 and ABI1 were coeluted at 14.0 ml, both in the presence and in the absence of ABA (Figure 2A, lower panels), indicating ligand-independent formation of a stable complex between PYL10 and ABI1. We further confirmed this interaction using surface plasmon resonance (SPR) analyses, in which ABI1 was immobilized onto the CM5 sensor chip. In the absence of ABA, PYL2 shows no detectable binding to ABI1. By contrast, PYL10 binds to ABI1 with a dissociation constant (K_d) of 1.2 μM. When preincubated with ABA, PYL2 exhibits a strong binding to ABI1 with a K_d of 0.25 μM, whereas ABA-incubated PYL10 shows an even stronger interaction with a K_d of 0.02 μM (Figure S2).

To further corroborate the notion that PYL10 constitutively associates with PP2C, we sought to obtain the structure of PYL10 in complex with PP2C in the absence of ABA. We attempted to cocrystallize PYL10 with various PP2Cs and eventually succeeded in crystallization of the PYL10-HAB1 complex. The structure was determined with molecular replacement and refined to 2.1 Å resolution with a free R factor of 0.207 (Table 1 and Figure 2B). The overall structure of PYL10-HAB1 complex closely resembles those of other PYL-PP2C complexes (Melcher et al., 2009; Miyazono et al., 2009; Yin et al., 2009). Notably and not surprisingly, the switch loop CL2 of PYL10 in the complex adopts a closed conformation as observed in the ABA-bound PYL2 (Figure 2C). The structure demonstrated unambiguously

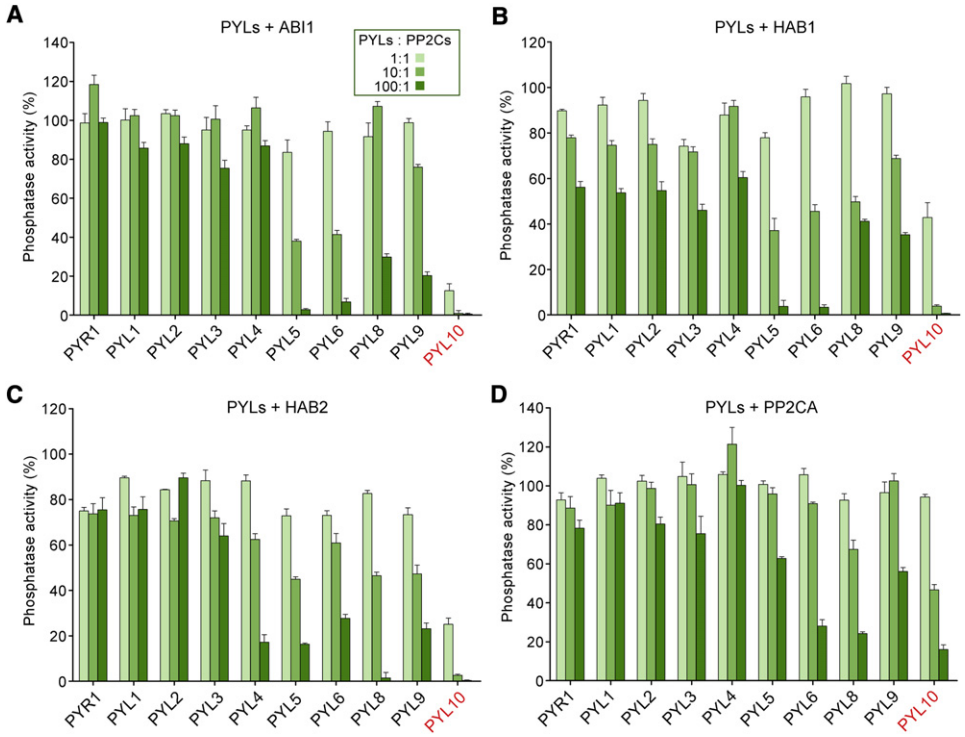

Figure 1. A Subclass of PYLs Inhibits PP2Cs in the Absence of ABA

The inhibitory effects on ABI1 (A), HAB1 (B), HAB2 (C), and PP2CA (D) by ten PYLs in the absence of ABA were measured. The details of the experiments are described in the Experimental Procedures. The readout of the reaction without phosphatase was set as baseline. The concentrations of PP2Cs are 0.4 μM for ABI1, 0.27 μM for HAB1, 0.67 μM for HAB2, and 0.3 μM for PP2CA. The concentrations of each PYL were set with molar ratios to PP2Cs as 1:1, 10:1, and 100:1 (color coded from light green to dark green), respectively. The relative phosphatase activity of each reaction was normalized against the reactions containing substrate, PP2Cs, and the loss-of-function variant of PYL2-S89R/S94R at three concentrations, respectively. The data before normalization are shown in Figure S1. Each reaction was repeated at least three times; error bars represent standard deviations. All the phosphatase assays were performed and presented in the same way throughout the manuscript.

See also Figure S1.

that PYL10 is able to form a stable complex with PP2C even in the absence of any ligand.

PYLs 4–10 Are Monomers in Solution

Previous structural investigations revealed that ABA is required to stabilize a closed conformation of the switch loop CL2 in PYR1, PYL1, and PYL2, such that a PP2C-interaction surface is created. PYL10, whose CL2 is already in a compatible conformation for PP2C binding in the absence of ABA as shown in the PYL10-HAB1 complex, thus represents a PYL subclass that is different from PYR1, PYL1, and PYL2. To understand the molecular basis of ABA-independent PP2C inhibition by PYL10, we performed in-depth structural and biochemical characterizations.

First we crystallized the ligand-free PYL10 in the space group $C222_1$, determined the structure by molecular replacement, and refined it to 1.5 Å resolution (Table 1). There is one PYL10 molecule in each asymmetric unit, while two symmetry-related molecules form a crystallographic dimer (Figure 3A). We had anticipated a closed CL2 conformation in the ligand-free PYL10, which would readily explain the constitutive inhibition of PP2C by PYL10. However, when the structure of ligand-free PYL10 protomer was superimposed with those of ligand-free PYL2 whose CL2 is in an open conformation, and HAB1-bound PYL10 whose CL2 is closed, it became obvious that CL2 in the ligand-free PYL10 closely resembles the open conformation (Figure 3B). Then why PYL10, but not PYL2, was able to bind to PP2C in the absence of ABA?

Our previous study showed that dimer formation of PYL2 was weakened upon ABA binding (Yin et al., 2009). Dimer formation of PYL2 may constrain CL2, which is heavily involved in the dimer interface, in an incompatible conformation for PP2C binding, and thus prevent the binding and inhibition of PP2C (Yin et al., 2009). Despite formation of a crystallographic dimer for PYL10, ligand-free PYL10 was eluted at 16.2 ml in SEC, which was consistent with the molecular mass of a single PYL10 molecule. By contrast, although PYL2 and PYL10 share similar calculated molecular weights (MWs) of 23.18 KDa and 23.07 KDa, the elution volume for PYL2 was approximately 1 ml ahead of PYL10 (Figure 2A) and consistent with the molecular mass of a PYL2 homodimer. These observations suggested that PYL10 may exist as a monomer in solution.

To further examine the oligomerization state of PYL10, we subjected the protein to both analytical ultracentrifugation (AUC) and static light scattering (SLS) analyses, with PYL2 as control. As anticipated, PYL2 exhibited a molecular mass of 45.9 ± 2.3 KDa as measured by AUC and 47.0 ± 0.1 KDa by

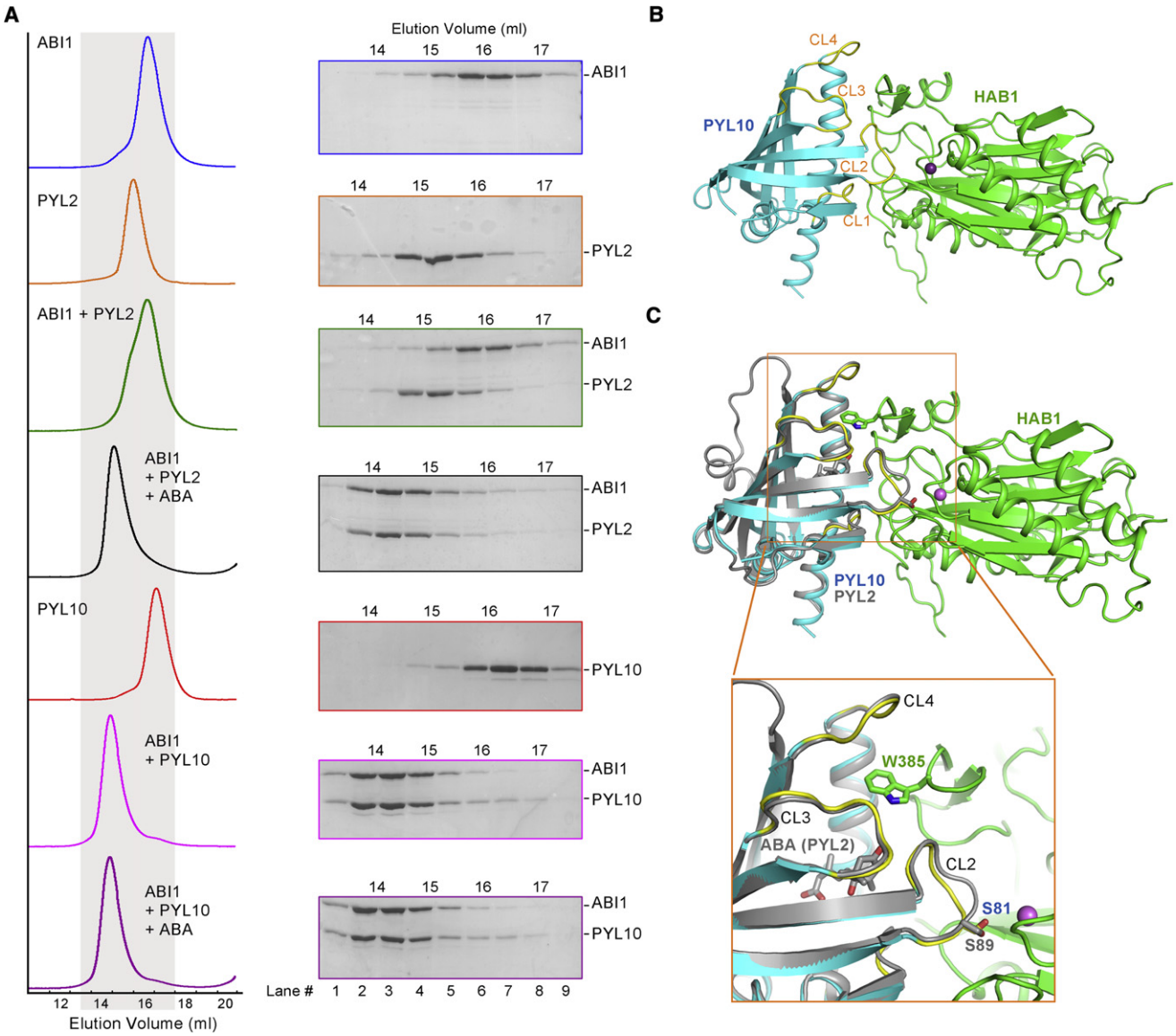

Figure 2. PYL10 and PP2Cs Form Stable Complex in the Absence of ABA

(A) SEC analyses of the interactions between ABI1 and PYL2/PYL10, in the presence or absence of ABA. The same elution fractions of each SEC injection were applied to SDS-PAGE followed by Coomassie blue staining.

(B) The overall structure of PYL10-HAB1 complex in the absence of ABA refined to 2.1 Å resolution. The four conserved loops, CL1–CL4, are highlighted in yellow. The metal ion is shown as purple sphere to indicate the active site of HAB1.

(C) The conformation of CL2 in the PYL10-HAB1 complex is identical to that of ABA-bound PYL2 (colored gray). The structure of ABA-bound PYL2 (PDB code 3KDI) was superposed to that of HAB1-bound PYL10. ABA in PYL2 was shown as gray sticks.

All structure figures were prepared with PyMol (DeLano, 2002). See also Figure S2.

SLS, which are close to the molecular mass of a PYL dimer. By contrast, the molecular weight of PYL10 was measured to be 19.7 ± 1.6 KDa and 26.3 ± 0.1 KDa, by AUC and SLS, respectively, which are consistent with that of a PYL monomer (Figures 3C and 3D and Table 2; see also Figure S3A). The oligomerization state of PYL10 remained unchanged with increasing protein concentrations (Figure S3B). Based on these observations, we conclude that PYL10 is a monomer in solution and the crystallographic dimer is likely a consequence of crystal packing.

This finding led us to re-examine the oligomerization states of the other PYLs, which showed distinct inhibitory effects on PP2Cs in the absence of ABA (Figure 1). We performed AUC and SLS analyses for all the available recombinant PYLs. While PYR1, PYL1 and PYL2 all displayed molecular weights corresponding to a dimer, PYL4 through PYL10 (except PYL7) exhibited molecular weights that are consistent with those of monomers (Table 2). The only exception is PYL3, which, with a calculated molecular weight of 25.18 KDa, exhibited

Table 1. Data collection and refinement statistics

	Ligand-Free PYL10+HAB1	Ligand-Free PYL10
Data Collection		
Space group	$P2_1$	$C222_1$
Cell dimensions		
a, b, c (Å)	70.77, 83.50, 88.54	38.017, 98.425, 96.718
α, β, γ (°)	90.00, 97.20, 90.00	90, 90, 90
Wavelength (Å)	1.0000	1.0000
Resolution (Å)	35–2.10 (2.18–2.10)	50–1.50 (1.55–1.50)
R_{merge} (%)	8.2 (39.9)	4.0 (37.8)
I / σI	16.1 (4.2)	45.1 (5.5)
Completeness (%)	99.8 (99.9)	99.7 (100.0)
Redundancy	3.9	7.4
Refinement		
Resolution (Å)	35–2.10	50–1.50
Number of reflections	58,037	29,479
R_{work} / R_{free} (%)	17.30 / 20.67	17.39 / 20.56
Number of atoms		
Protein	7730	1456
Ligand/ion	2	0
Water	507	176
B factors		
Protein	36.11	28.54
Ligand/ion	18.25	0
Water	39.09	38.99
Rmsds		
Bond lengths (Å)	0.008	0.007
Bond angles (°)	1.129	1.123
Ramachandran plot statistics (%)		
Most favored	89.4	90.5
Additional allowed	10.6	9.5
Generously allowed	0.0	0.0
Disallowed	0.0	0.0

One crystal was used for each structure. Values in parentheses are for the highest-resolution shell. $Rmerge = \Sigma h \Sigma i |Ih,i - Ih| / \Sigma h \Sigma i Ih,i$, where Ih is the mean intensity of the i observations of symmetry related reflections of h. $R = \Sigma |Fobs - Fcalc| / \Sigma Fobs$, where $Fcalc$ is the calculated protein structure factor from the atomic model (R_{free} was calculated with 5% of the reflections selected randomly).

a molecular mass of 33.0 ± 0.1 KDa by AUC and 34.1 ± 3.0 KDa by SLS. This could result from a fast equilibrium between a monomer and a dimer. Notably, PYR1 and PYLs 1–3 depend on ABA for the inhibition of PP2Cs, whereas PYLs 4–10 inhibited PP2Cs to various extents without ABA. These observations substantiate the notion that dimer formation of PYLs prevents the inhibition of PP2Cs in the absence of ABA (Yin et al., 2009).

Engineering of a Monomeric PYL2

The existence of monomeric PYLs provides an appealing explanation to the constitutive inhibition of PP2C. It is noteworthy that CL2 was located on the interface of the crystallographic dimer of PYL10. Hence, the observed open conformation of CL2 may be a result of crystallization and may be different from that in solution (Figure 3A). In the absence of the constraint from an adjacent protomer, CL2 of the monomeric PYL10 is likely to be flexible in solution and thus able to adopt a compatible conformation for PP2C recognition even in the absence of ABA. This notion was supported by nuclear magnetic resonance analyses (C. Tian, personal communication).

PYL10 and PYL2 share a sequence identity of 45% and similarity of 66% over 167 amino acids (Figure S4). To understand why PYL2 exists as a dimer while PYL10 is a monomer, we scrutinized the dimer interface of PYL2 as well as the sequence differences between PYL2 and PYL10. Previous studies showed that a mutant of PYL2 containing five point mutations (F66A, I88A, N157A, M164A, and F165A) disrupted the dimer formation (Yin et al., 2009). Sequence alignment shows that among these five amino acids, only Ile88 and Met164 are altered in PYL10, with Ile88 replaced by Lys80 and Met164 by Phe154 (Figure S4). Given that both Met and Phe are hydrophobic residues, the difference between Ile and Lys may play a more prominent role in determining their different oligomerization states. A closer examination of the dimer interface of the two PYLs confirmed this analysis. In PYL2, Ile88 packs against two hydrophobic amino acids, Met164 and Phe165, of the other protomer (Figure 4A, left panel). In PYL10, where Ile88 is replaced by the corresponding residue Lys80, the van der Waals interactions are partially disrupted. Yet Lys80 is surrounded by hydrophobic residues Phe154 and Phe155 of the adjacent molecule (Figure 4A, right panel). This structural organization may impede dimer formation in solution. To support the structural analysis, we generated a PYL2 variant with single point mutation I88K and examined its oligomeric state by SEC. PYL2-I88K exhibited an elution volume that is approximately 1 ml slower than WT PYL2 (Figure 4B), suggesting that PYL2-I88K exists as a monomer in solution.

We measured the binding affinity of PYL2-I88K toward ABA using isothermal titration calorimetry (ITC) and examined its ability to inhibit PP2Cs in response to ABA. PYL2-I88K binds to ABA with an apparent dissociation constant (K_d) of 8.2 ± 1.1 μM, which is approximately 7-fold tighter than in the case of WT PYL2 (Figure 4C). In addition, PYL2-I88K completely inhibited the phosphatase activities of the four PP2Cs in the presence of ABA (Figure 4D). Therefore, PYL2-I88K is a functional variant.

Then we examined whether the monomeric PYL2-I88K was able to inhibit PP2Cs in the absence of a ligand. The assay was performed according to the same protocol as for the WT PYLs. PYL2-I88K exhibited an increased constitutive inhibition of PP2Cs compared to WT PYL2 (Figure 4E; see also Figure S5). For example, at a concentration of about 4 μM, PYL2-I88K suppressed approximately 65 percent of the phosphatase activity of HAB1 in the absence of ABA. Nonetheless, the inhibitory effect was much weaker than that of PYL10, suggesting that other elements may also contribute to the ABA-independent inhibition of PP2Cs by PYLs.

Identification of Second Molecular Determinant for the Constitutive Activity of PYLs

To identify other factors of PYLs that contribute to the ABA-independent inhibition of PP2Cs, we thoroughly examined the

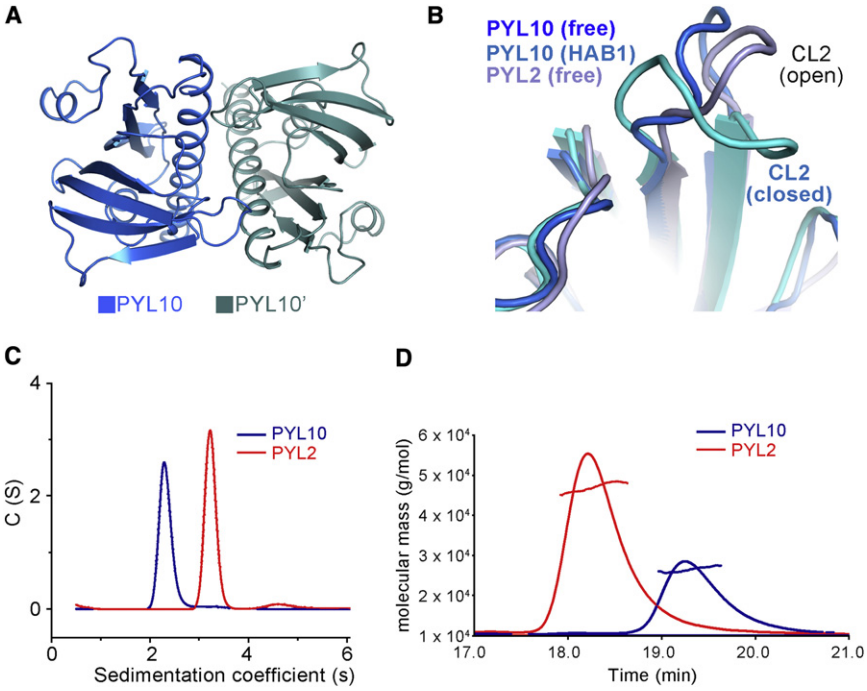

Figure 3. PYL10 Is a Monomer in Solution

(A) The overall structure of the ligand-free PYL10 refined at 1.5 Å resolution. There is one molecule of PYL10 in each asymmetric unit. Two molecules from adjacent asymmetric units, which form a crystallographic dimer, are shown.

(B) Structural superimposition of the ligand-free PYL10 with HAB1-bound PYL10 and ligand-free PYL2 revealed an open conformation of the CL2 in the ligand-free PYL10.

(C) Molecular mass of PYL10 and PYL2 measured by sedimentation velocity (AUC).

(D) Molecular mass of PYL10 and PYL2 measured by static light scattering (SLS).

See also Figure S3.

available structures. Binding to and inhibition of PP2Cs require closure of the switch loop CL2. The ligand-binding pocket of PYLs is hydrophilic and filled with water molecules, whereas the pocket-facing side of CL2 contains mostly hydrophobic amino acids. Therefore, the role of the ligands, ABA and pyrabactin (Hao et al., 2010; Melcher et al., 2010a; Peterson et al., 2010; Yuan et al., 2010), which are both amphipathic, is probably to "neutralize" the polarity of the pocket and to dock the hydrophobic side of CL2. In the case of PYL10, the closure of CL2 in the absence of a ligand may be achieved through the stable hydrophobic interactions between the ligand-free pocket and CL2. Based on this analysis, we carefully analyzed the sequence alignment of PYLs, particularly the residues that may form contacts with residues in CL2. A good candidate is Leu79 of PYL10, which demarcates strand β3 and CL2. Notably, in all other 12 PYLs, this position is occupied by a valine residue (Figure 5A).

To examine whether substitution of leucine by valine would affect constitutive inhibition of PP2Cs, we generated a PYL2 variant V87L. While PYL2-V87L slightly reduced the phosphatase activities of HAB2 and PP2CA, it exhibited considerable inhibitory effect on ABI1 and HAB1. When added in 100-fold excess, PYL2-V87L inhibited up to 60%–70% of the phosphatase activities of ABI1 and HAB1, an effect similar to that of PYL2-I88K (Figure 5B; see also Figure S5). To understand the molecular basis underlying the stronger constitutive inhibition of PP2Cs by PYL2-V87L, we compared the coordination of CL2 in the structure of ABA-bound PYL2 to that of HAB1-bound PYL10, both of which are in the closed conformation (Figure 5C, left panel). In PYL10, the side chain of Leu79 makes van der Waals contacts with Leu83 and Ala85 in CL2 and Ile59 in CL1. Adding to this network of interaction is Leu159 in helix α2, which contacts Leu83 in CL2. The network formed by hydrophobic residues may effectively anchor CL2 to a closed conformation (Figure 5C, central panel). Notably, PYLs 4–12 contain either leucine or isoleucine at the position corresponding to Leu159 in PYL10, whereas PYR1 and PYLs 1–3 have a valine instead (Figure S4). In the case of PYL2, a Val87 is located at the corresponding position of Leu79 in PYL10. It makes far fewer interactions with surrounding hydrophobic residues. The only van der Waals contacts are made between Val87 and Leu91/Ala93 in CL2 (Figure 5C, right panel). Therefore, in the absence of an amphipathic ligand, CL2 of PYL2 may not favor a closed conformation, even for the monomeric mutant PYL2-I88K.

Our biochemical and structural analyses collectively support the notion that bulkier hydrophobic residues at the entrance to the ligand-binding pocket provide a platform to dock the pocket-facing, hydrophobic side of CL2, thus facilitating a closed conformation of CL2.The substitution of Val87 by Leu in PYL2 helps stabilize the closed conformation of CL2, whereas the mutation I88K makes PYL2 a monomer. A PYL2 variant

Table 2. The Molecular Weight of PYL Proteins Measured by Static Light Scattering and Analytical Ultracentrifugation

Protein	MW-KDa (Theoretical)	MW-KDa SLS	MW-KDa AU	Model Fitting
PYR1	24.37	48.0 ± 0.2	48.8 ± 2.2	dimer
PYL1	27.26	56.3 ± 0.2	57.0 ± 2.0	dimer
PYL2	23.18	47.0 ± 0.1	45.9 ± 2.3	dimer
PYL3	25.18	33.0 ± 0.1	34.1 ± 3.0	monomer-dimer
PYL4	24.33	27.4 ± 0.1	22.2 ± 1.9	monomer
PYL5	24.56	28.3 ± 0.1	26.5 ± 2.0	monomer
PYL6	25.74	29.4 ± 0.1	23.0 ± 2.6	monomer
PYL8	25.74	26.9 ± 0.2	22.8 ± 2.3	monomer
PYL9	22.80	27.7 ± 0.1	20.3 ± 1.9	monomer
PYL10	23.07	26.3 ± 0.1	19.7 ± 1.6	monomer

See also Figure S4.

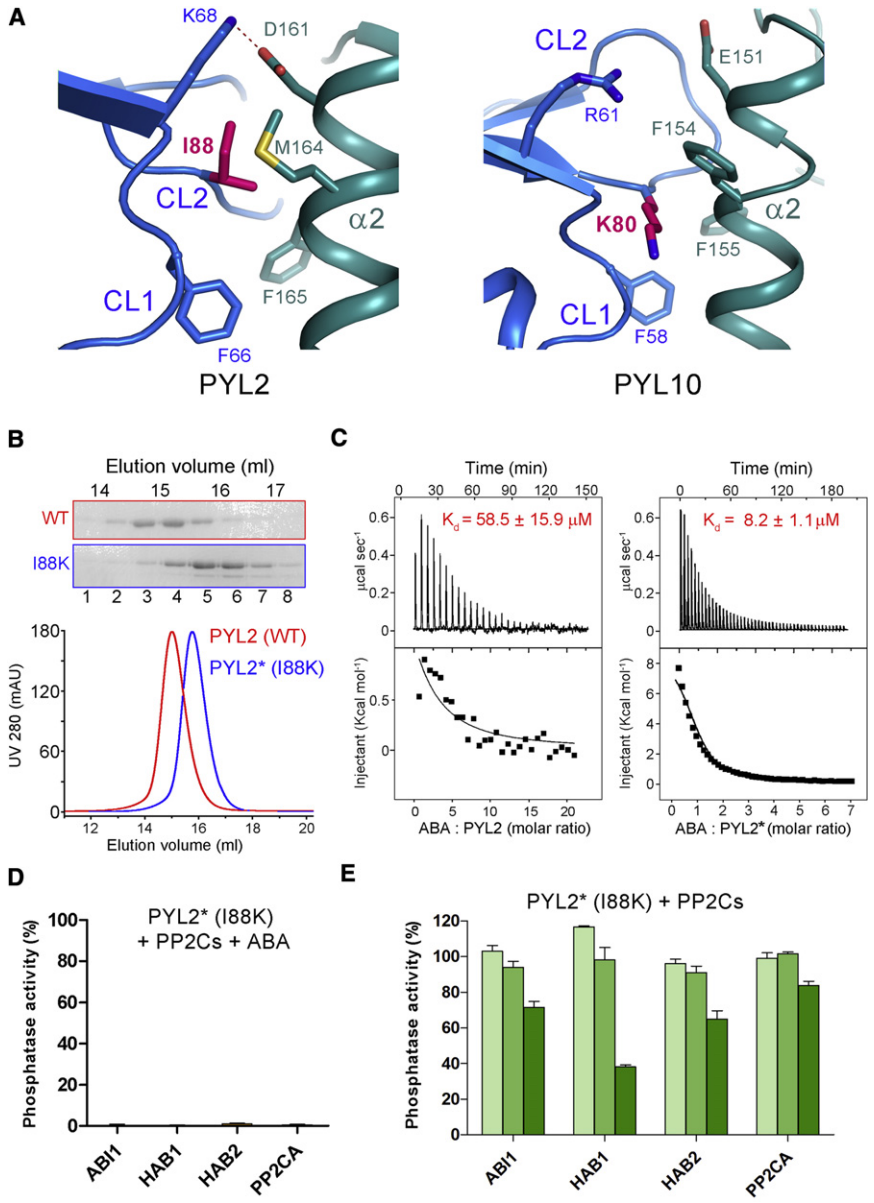

Figure 4. Monomeric Variant of PYL2 Obtained Weak Constitutive Activity

(A) PYL10 has an unfavorable dimer packing in the crystal structure. Left: The van der Waals contacts between the ligand-free PYL2 dimer mediated by Ile88 and surrounding hydrophobic residues. Right: The dimer interface surrounding K80 between the ligand-free PYL10 molecules in the crystal structure.

(B) PYL2-I88K is a monomer in solution. The WT and PYL2-I88K were subjected to SEC, and the peak fractions were taken for SDS-PAGE followed by Coomassie blue staining.

(C) PYL2-I88K has a higher apparent binding affinity with ABA than WT PYL2. The binding affinity between ABA and PYL2 variants was measured by ITC. The curve was fit by Origin 7.0.

(D) PYL2 -I88K is a functional variant. The phosphatase activities of four PP2Cs were completely inhibited by 4 μM PYL2-I88K in the presence of 10 μM ABA.

(E) PYL2-I88K exhibits weak inhibition of PP2Cs in the absence of ABA. The assay was performed according to the same protocol as for the WT PYLs. Each reaction was repeated for at least three times; error bars represent standard deviations.

See also Figure S5.

containing both of point mutations is predicted to exhibit a stronger inhibitory effect than either variant alone. To test this idea, we generated the double mutant PYL2-V87L/I88K. With PYL2-V87L/I88K added in 100-fold excess, the phosphatase activity of HAB1 was nearly abrogated, while that of ABI1 was reduced by approximately 80% (Figure 5D; see also Figure S5). Although the inhibition of HAB2 and PP2CA was not as significant as ABI1 or HAB1, it was apparent that PYL2-V87L/I88K exhibited a stronger inhibitory effect than either PYL2-V87L or PYL2-I88K (Figure S5).

DISCUSSION

In this study, we identified a subclass of PYLs, exemplified by PYL10, which exhibits ABA-independent inhibition of PP2Cs (Figure 5E). These observations are consistent with the reported Y2H results in which PYLs 5–12, except the untested PYL8, were shown to interact with HAB1 in the absence of ligand (Park et al., 2009). In addition, PYL10 was shown to partially inhibit ABI1 in the absence of ABA in the protoplast (Fujii et al., 2009). Structural and biochemical characterizations revealed two molecular determinants that contribute to ABA-independent inhibition of PP2Cs by PYLs. First, a monomeric state of PYLs appears to be necessary for the constitutive association with and inhibition of PP2Cs (Figure 5E). However, being a monomer appears to be a necessary, but not sufficient, condition for PYLs to be able to constitutively inhibit PP2Cs. Further examinations revealed a second determinant, that is, the residues guarding the ligand-binding pocket of PYLs must be bulky and hydrophobic so that they can make sufficient hydrophobic contacts to stabilize a closed CL2 (Figure S6). If the biochemical features of a PYL pocket do not match those of the CL2, then an amphipathic ligand, such as ABA or pyrabactin, is required to bridge the gap between the pocket and CL2 (Figure 5E; see also Figure S6).

Notably, the monomeric mutant PYL2-I88K exhibited a binding affinity with ABA about 7-fold higher than that of WT PYL2 (Figure 4C). When measured by ITC, the apparent K_d may reflect the free energy change of three processes: binding of ABA to the pocket residues, conformational rearrangement of CL2, and

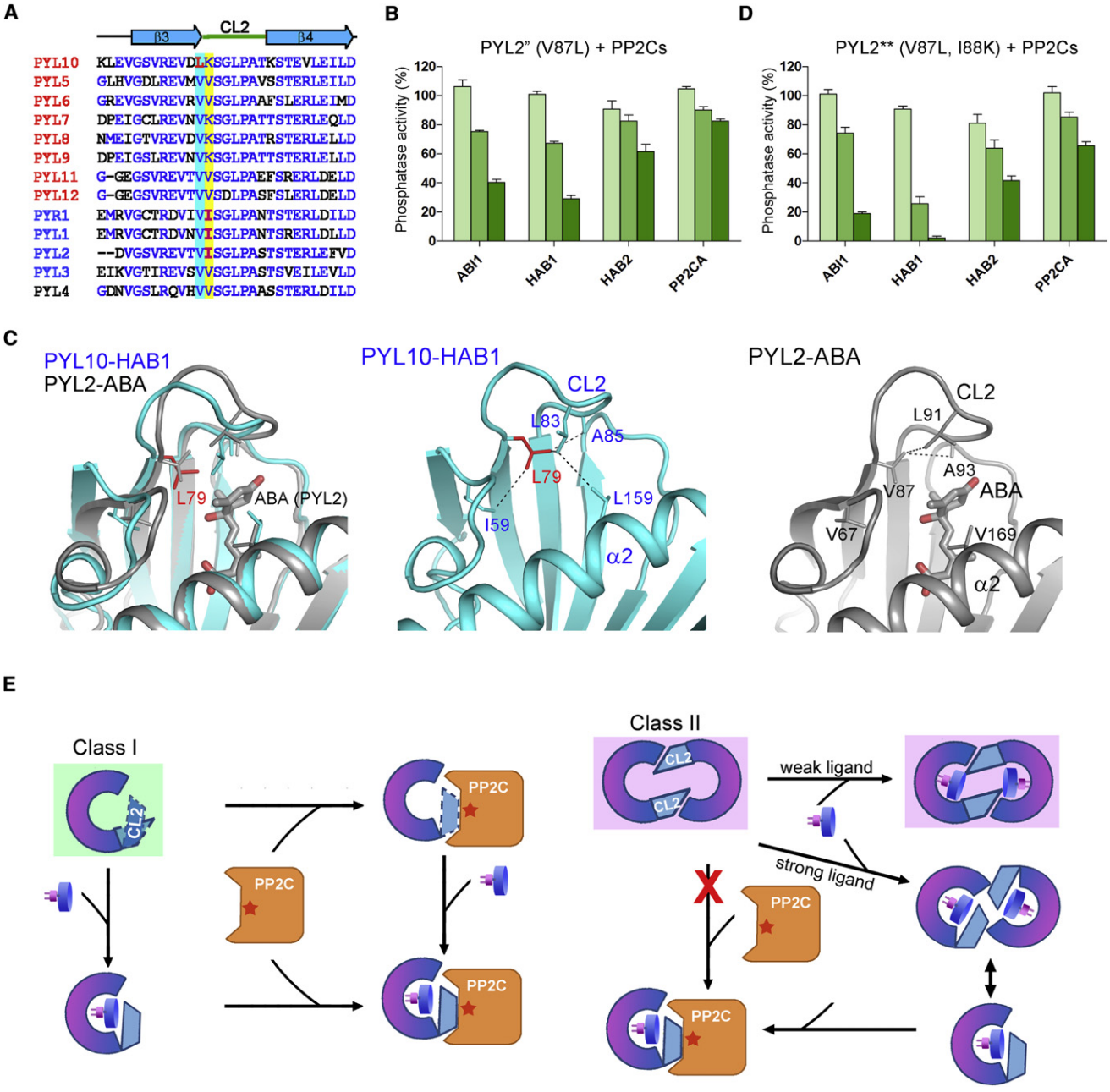

Figure 5. Identification of a Second Determinant of PYLs for ABA-Independent Inhibition

(A) Sequence alignment revealed that only PYL10 contains a leucine that demarcates β3 and CL2, whereas a valine is present at the corresponding position in all other ABA-responsive PYLs.

(B) PYL2-V87L gained weak constitutive inhibition of PP2Cs.

(C) Structural comparison of HAB1-bound PYL10 and ABA-bound PYL2. Left: Structural superposition of HAB1-bound PYL10 (cyan) and ABA-bound PYL2 (gray). The ABA molecule in PYL2 is shown as gray sticks. Middle: Leu79 is at the center of a network of van der Waals contacts constituted of residues from CL2, CL1, and α2 in PYL10. Right: There is far fewer van der Waals contact between the hydrophobic residues of CL2 and the residues in other part of PYL2.

(D) PYL2-V87L/I88K exhibited a stronger constitutive inhibition of PP2Cs than either of PYL2-V87L or PYL2-I88K. A different way of data presentation is shown in Figure S5 to compare the inhibitory effects of WT and mutant PYL2 proteins on each PP2C. Each reaction was repeated for at least three times; error bars represent standard deviations.

(E) Classification of PYLs based on their oligomerization states. Left: Class I PYLs are monomers. They may bind and inhibit PP2Cs in the absence of a ligand because the switch loop CL2 retains the flexibility to adopt a compatible conformation for binding to PP2Cs. Right: Class II PYLs are dimers. PYR1 and PYLs 1–3 rely on ligand for PP2C binding and inhibition. ABA, the "strong" ligand, is a suitable ligand for all the PYLs. By contrast, pyrabactin represents a "weak" ligand in that it can bind to but cannot induce the conformational change of CL2 in PYL2 (Peterson et al., 2010; Yuan et al., 2010).

See also Figures S5 and S6.

splitting of the homodimeric interface of PYL in the case of a dimer. While binding of ABA is energetically favorable, the rearrangement of the homodimer might be energy consuming (Figure S6A). Accordingly, given generally similar biochemical features, monomeric PYLs, which do not require extra energy to rearrange the dimer, might exhibit a tighter apparent affinity than dimeric PYLs. Under these circumstances, the monomeric PYLs may be more sensitive to ABA signal than the dimeric PYLs.

Our study also revealed the distinct recognition specificities between various PYLs and PP2Cs. ABA-bound PYL10 binds to ABI1 with a binding affinity (K_d = 18.2 nM) approximately 15-fold higher than ABA-bound PYL2 (K_d = 252 nM) (Figure S2E). Interestingly, ABA-bound PYL2 and PYL10 exhibit similar k_{on}, but distinct k_{off} values for the binding to ABI1 (Figure S2E), indicating that the complex of PYL10-ABA-ABI1 is more stable than that of PYL2-ABA-ABI1. This observation may be explained by the fact that ABA-bound PYL2 is at equilibrium between the formation of homodimer and the heterodimeric association with ABI1. In addition, the in vitro examinations revealed that ligand-free PYLs 4–10 exhibited distinct inhibitory effects on different PP2Cs (Figure 1). The existence of seemingly redundant but functionally diverse PYLs may collectively provide a quantitative and thus more accurate and sensitive regulation system of the phosphatase activity of PP2Cs.

Our biochemical and structural investigations also raise a number of questions. What is the physiological significance of the ABA-independent PYLs? One possibility is that PYLs 4–10 might be involved in processes other than ABA responses. As PYLs are a family of proteins identified only recently, it remains to be investigated whether PYLs are only acting in the ABA signaling pathway. The finding reported here suggests that a subset of PYL might have ABA-independent functions. This divergence leads to a more interesting question of at which point in evolution ABA became a stress hormone for plants. It could be that PYLs were evolved to be a functional phosphatase inhibitor before ABA was used as hormone. After gene duplication and divergence, some of the members might adopt the ability to bind to ABA and eventually evolve into ABA receptors. An alternative implication of this finding may be that ABA, as a stress hormone, is so essential for plants that even when the ABA level is completely depleted due to genetic mutations or environmental disturbances, the constitutive activity of PYLs 4–10 might ensure a basal level of ABA signaling in operation for plant survival and growth. A related question then is how to release the inhibition of PP2Cs exerted by either the constitutively active or ABA-bound PYLs. Are there more modulators that might disrupt the complex between PYLs and PP2Cs, or the PYLs may be subject to posttranslational modifications? These interesting questions remain to be addressed. Our study provides an important framework for the future investigations.

Our findings also shed light on the potential applications of these constitutively active receptors. By knowing the molecular mechanism of the ABA-independent feature, we may engineer PYLs for enhanced and constitutive activity as ABA receptors. Such variants would be useful in agriculture, particularly for generation of transgenic crops with enhanced ABA sensitivity to tolerate environmental stresses.

EXPERIMENTAL PROCEDURES

Protein Preparation and Crystallization

All PYR/PYLs homologs, ABI1 (AT4G26080), HAB1 (AT1G72770), HAB2 (AT1G17550), and PP2CA (AT3G11410) were subcloned from the *Arabidopsis thaliana* complementary DNA library using standard PCR-based protocol. All mutants of PYLs were generated with two-step PCR and verified by plasmid sequencing. All the proteins were purified according the protocol described previously (Yin et al., 2009). So that individual protein for activity assay or crystallization could be obtained, PYLs and PP2Cs were subcloned into pET-15b and overexpressed in *E. coli* strain BL21(DE3). Protein expression was induced at 22°C for 12 hr. The proteins were purified with Ni-NTA resin (QIAGEN), followed by anion exchange chromatography (Source-15Q, GE Healthcare) and size-exclusion chromatography (Superdex-200, GE Healthcare). For obtainment of the PYL10-HAB1 complex, PYL10 subcloned into vector pBB75 and HAB1 in pET15b, were coexpressed in *E. coli* strain BL21(DE3) and purified according to the protocol described above.

Before crystallization, the His-tag of PYL10 protein or PYL10 (1–183)-HAB1 (172–511) binary complex was removed by thrombin digestion. Crystals were grown at 18°C via the hanging-drop vapor-diffusion method. Typical crystals of ligand-free PYL10 appeared after 3 to 4 days in the well buffer containing 0.2 M magnesium acetate and 20% PEG3350. The crystals of PYL10-HAB1 binary complex appeared in the well-buffer containing 100 mM Tris (pH 8.0), 21% PEG3350, and 2% dioxane.

Data Collection, Structure Determination, and Refinement

The diffraction data were collected at either Shanghai Synchrotron Radiation Facility (SSRF) or SPring-8 in Japan, integrated and scaled with HKL2000 package (Otwinowski and Minor, 1997). Further data processing was carried out with programs from the CCP4 suite (Collaborative Computational Project, Number 4, 1994).

For determination of the structure of ligand-free PYL10, PYL2 (PDB code 3KDH) was selected as the molecular replacement model. So that a more accurate model could be made, the program Chainsaw (Stein, 2008) was applied to make a modification of the PYL2 structure. The sequence alignment between PYL10 and PYL2 was used as an input to Chainsaw. This newly modified structure was used as the initial model for molecular replacement. The structure of the newly refined ligand-free PYL10 and that of HAB1 extracted from the ABA-PYL2-HAB1 complex (PDB code 3NMT) were used as initial models for the structural determination of PYL10-HAB1 binary complex. Both of the molecular replacements were performed with program PHASER (McCoy et al., 2007), and manual model rebuilding and refinement were iteratively performed with COOT (Emsley and Cowtan, 2004) and PHENIX (Adams et al., 2002). Data collection and refinement statistics are summarized in Table 1.

Isothermal Titration Calorimetry Assays

The ITC experiments were performed with VP-ITC Microcalorimeter (MicroCal). Thermodynamic constants were determined by Origin 7.0 (Origen Laboratories). (+)-ABA (1 mM; Sigma Aldrich) was dissolved in the reaction buffer containing 20 mM HEPES (pH 7.5), and 150 mM NaCl was titrated against 10 μM PYL variants purified in the same buffer. The stoichiometry between ligand and protein was set to 1 for all analyses.

Phosphatase Activity Assay

The phosphatase activity was measured by the Ser/Thr phosphatase assay system (Promega). The protocol of phosphatase activity assay was described previously with some modifications (Yin et al., 2009). Each reaction was performed in a 50 μl reaction volume. The concentrations of the phosphatases (0.4 μM ABI1, 0.27 μM HAB1, 0.67 μM HAB2, and 0.3 μM PP2CA) were adjusted so that the readout of the assay is within the linear range of the absorbance measurement. The concentrations of PYLs proteins were adjusted so as to match the molar ratios indicated in the manuscript. 10 μM (+)-ABA was added if required. After incubation with peptide substrate (supplied with the Promega kit) in 50 mM imidazole (pH 7.2), 5 mM $MgCl_2$, 0.2 mM EGTA, and 0.1 mg/ml BSA at 30°C for 20 min, the reaction was stopped by addition of 50 μl molybdate dye. After incubation for another 15 min at room temperature,

absorbance at 630 nm was measured. The readout of the reaction without phosphatase was set as baseline and the value was subtracted from all the assay data. All the data are means ± standard deviation from at least three independent experiments.

Size-Exclusion Chromatography

The SEC analyses were performed with a SD200 (Superdex-200 HR10/30, GE Healthcare) in the buffer containing 20 mM HEPES (pH 7.5), and 150 mM NaCl. For examination of the oligomerization state of PYLs proteins or interaction with PP2Cs, 400 μl PYL proteins (OD_{280} = 0.65) or protein mixtures (approximately 17 μM each) were individually applied to SD200. In the test requiring ABA, 0.4 mM ligand was incubated with the proteins before injection.

Static light scattering measurements

SLS measurements were performed at 18°C on a DAWN HELEOS II instrument (Wyatt Technology, Santa Barbara, CA). All PYLs proteins were diluted to 1.0 mg/ml in the reaction buffer containing 20 mM HEPES (pH 7.5) and 150 mM NaCl for SLS analyses. Calibration of the light scattering detector was verified with albumin monomer standard before the assays. The data was analyzed with ASTRA software (Wyatt Technology, version 5.3.4.11).

Analytical Ultracentrifugation Analyses

Sedimentation velocity was performed with an XL-I analytical ultracentrifuge (Beckman Coulter) equipped with a four-cell An-60 Ti rotor at 20°C. Reaction buffer containing 20 mM HEPES (pH 7.5) and 150 mM NaCl was used as the reference solution. All PYLs proteins (OD_{280} = 0.85) were applied at a speed of 60,000 rpm. Absorbance scans were taken at 280 nm at the intervals of 0.003 cm size in a radical direction. The differential sedimentation coefficients, c(s), frictional coefficients, and molecular weight were calculated by ProteomeLab software (Beckman Coulter).

Surface Plasmon Resonance Analyses

The SPR experiments were carried out on a Biacore T100 (GE Healthcare). The ABI1 protein was dissolved in the coupling buffer (20 μg/ml in 10 mM sodium acetate [pH 5.5]) and immobilized onto the CM5 sensor chip at 2722 response unit (RU) with the coupling reagents of 0.2 M N-ethyl-N'-(3-dimethylaminopropyl) carbodiimide (EDC) and 50 mM N-hydroxysuccinimide (NHS) based on the standard primary amine-coupling procedure. HBS-P, which contains 10 mM HEPES, 150 mM NaCl, 0.005% (v/v) surfactant P_{20}, was used as the running buffer. Equilibration of the baseline was performed by a continuous flow of HBS-P buffer through the chip surface for 1 to 2 hr. The sensorgram was then collected at 25°C with HBS-P as the running buffer at a constant flow of 30 μl/min to determine the binding affinity. Each protein (as the analyte) was serially diluted by 3-fold with the running buffer, having the highest final concentration at 20 μM. The diluted samples were injected into the channels for 120 s, followed by washing for more than 120 s with the running buffer. The equilibrium dissociation constant (K_d) and the association (k_{on}) and dissociation (k_{off}) rate constants were determined by Equations 1 and 2:

$$K_d = k_{off}/k_{on} \quad (1)$$

$$\frac{dR}{dt} = k_{on} \times C \times (R_{max} - R) - k_{off} \times R, \quad (2)$$

where R is the RU number and C is the concentration of the analyte. The curve fitting efficiency is evaluated by a statistical parameter χ^2.

ACCESSION NUMBERS

Coordinates and structure factor amplitudes have been deposited in the Protein Data Bank with accession numbers 3RT0 and 3RT2.

SUPPLEMENTAL INFORMATION

Supplemental Information includes six figures and can be found with this article online at doi:10.1016/j.molcel.2011.05.011.

ACKNOWLEDGMENTS

We thank C. Tian at University of Science and Technology of China for providing the unpublished data. We thank X. Yu at the Institute of Biophysics, Chinese Academy of Sciences, for technical support with AUC and SLS analyses. We thank J. He and S. Huang at Shanghai Synchrotron Radiation Facility (SSRF) and N. Shimizu, S. Baba and T. Kumasaka at the Spring-8 beamline BL41XU for onsite assistance. We thank H. Guo (Peking University) and L. Yu (Tsinghua University) for critically reading the manuscript. This work was supported by funds from the Ministry of Science and Technology (grant numbers 2009CB918802 and 2011CB910501), Projects 91017011 and 31070644 of the National Natural Science Foundation of China, Tsinghua University 985 Phase II funds, and the Yuyuan Foundation.

Received: November 26, 2010
Revised: March 18, 2011
Accepted: May 20, 2011
Published: June 9, 2011

REFERENCES

Adams, P.D., Grosse-Kunstleve, R.W., Hung, L.W., Ioerger, T.R., McCoy, A.J., Moriarty, N.W., Read, R.J., Sacchettini, J.C., Sauter, N.K., and Terwilliger, T.C. (2002). PHENIX: building new software for automated crystallographic structure determination. Acta Crystallogr. D Biol. Crystallogr. *58*, 1948–1954.

Collaborative Computational Project, Number 4. (1994). The CCP4 suite: programs for protein crystallography. Acta Crystallogr. D Biol. Crystallogr. *50*, 760–763.

Cutler, S.R., Rodriguez, P.L., Finkelstein, R.R., and Abrams, S.R. (2010). Abscisic acid: emergence of a core signaling network. Annu. Rev. Plant Biol. *61*, 651–679.

DeLano, W.L. (2002). The PyMOL Molecular Graphics System. http://www.pymol.org.

Emsley, P., and Cowtan, K. (2004). Coot: model-building tools for molecular graphics. Acta Crystallogr. D Biol. Crystallogr. *60*, 2126–2132.

Fedoroff, N.V. (2002). Cross-talk in abscisic acid signaling. Sci. STKE *2002*, re10.

Finkelstein, R., Reeves, W., Ariizumi, T., and Steber, C. (2008). Molecular aspects of seed dormancy. Annu. Rev. Plant Biol. *59*, 387–415.

Fujii, H., Chinnusamy, V., Rodrigues, A., Rubio, S., Antoni, R., Park, S.Y., Cutler, S.R., Sheen, J., Rodriguez, P.L., and Zhu, J.K. (2009). In vitro reconstitution of an abscisic acid signalling pathway. Nature *462*, 660–664.

Hao, Q., Yin, P., Yan, C., Yuan, X., Li, W., Zhang, Z., Liu, L., Wang, J., and Yan, N. (2010). Functional mechanism of the abscisic acid agonist pyrabactin. J. Biol. Chem. *285*, 28946–28952.

Hubbard, K.E., Nishimura, N., Hitomi, K., Getzoff, E.D., and Schroeder, J.I. (2010). Early abscisic acid signal transduction mechanisms: newly discovered components and newly emerging questions. Genes Dev. *24*, 1695–1708.

Iyer, L.M., Koonin, E.V., and Aravind, L. (2001). Adaptations of the helix-grip fold for ligand binding and catalysis in the START domain superfamily. Proteins *43*, 134–144.

Klingler, J.P., Batelli, G., and Zhu, J.K. (2010). ABA receptors: the START of a new paradigm in phytohormone signalling. J. Exp. Bot. *61*, 3199–3210.

Ma, Y., Szostkiewicz, I., Korte, A., Moes, D., Yang, Y., Christmann, A., and Grill, E. (2009). Regulators of PP2C phosphatase activity function as abscisic acid sensors. Science *324*, 1064–1068.

McCoy, A.J., Grosse-Kunstleve, R.W., Adams, P.D., Winn, M.D., Storoni, L.C., and Read, R.J. (2007). Phaser crystallographic software. J. Appl. Cryst. *40*, 658–674.

Melcher, K., Ng, L.M., Zhou, X.E., Soon, F.F., Xu, Y., Suino-Powell, K.M., Park, S.Y., Weiner, J.J., Fujii, H., Chinnusamy, V., et al. (2009). A gate-latch-lock mechanism for hormone signalling by abscisic acid receptors. Nature *462*, 602–608.

Melcher, K., Xu, Y., Ng, L.M., Zhou, X.E., Soon, F.F., Chinnusamy, V., Suino-Powell, K.M., Kovach, A., Tham, F.S., Cutler, S.R., et al. (2010a).

Identification and mechanism of ABA receptor antagonism. Nat. Struct. Mol. Biol. *17*, 1102–1108.

Melcher, K., Zhou, X.E., and Xu, H.E. (2010b). Thirsty plants and beyond: structural mechanisms of abscisic acid perception and signaling. Curr. Opin. Struct. Biol. *20*, 722–729.

Miyazono, K., Miyakawa, T., Sawano, Y., Kubota, K., Kang, H.J., Asano, A., Miyauchi, Y., Takahashi, M., Zhi, Y., Fujita, Y., et al. (2009). Structural basis of abscisic acid signalling. Nature *462*, 609–614.

Nishimura, N., Hitomi, K., Arvai, A.S., Rambo, R.P., Hitomi, C., Cutler, S.R., Schroeder, J.I., and Getzoff, E.D. (2009). Structural mechanism of abscisic acid binding and signaling by dimeric PYR1. Science *326*, 1373–1379.

Nishimura, N., Sarkeshik, A., Nito, K., Park, S.Y., Wang, A., Carvalho, P.C., Lee, S., Caddell, D.F., Cutler, S.R., Chory, J., et al. (2010). PYR/PYL/RCAR family members are major in-vivo ABI1 protein phosphatase 2C-interacting proteins in Arabidopsis. Plant J. *61*, 290–299.

Otwinowski, Z., and Minor, W. (1997). Processing of X-ray diffraction data collected in oscillation mode. Methods Enzymol. *276*, 307–326.

Park, S.Y., Fung, P., Nishimura, N., Jensen, D.R., Fujii, H., Zhao, Y., Lumba, S., Santiago, J., Rodrigues, A., Chow, T.F., et al. (2009). Abscisic acid inhibits type 2C protein phosphatases via the PYR/PYL family of START proteins. Science *324*, 1068–1071.

Peterson, F.C., Burgie, E.S., Park, S.Y., Jensen, D.R., Weiner, J.J., Bingman, C.A., Chang, C.E.A., Cutler, S.R., Phillips, G.N., Jr., and Volkman, B.F. (2010). Structural basis for selective activation of ABA receptors. Nat. Struct. Mol. Biol. *17*, 1109–1113.

Santiago, J., Dupeux, F., Round, A., Antoni, R., Park, S.Y., Jamin, M., Cutler, S.R., Rodriguez, P.L., and Márquez, J.A. (2009a). The abscisic acid receptor PYR1 in complex with abscisic acid. Nature *462*, 665–668.

Santiago, J., Rodrigues, A., Saez, A., Rubio, S., Antoni, R., Dupeux, F., Park, S.Y., Márquez, J.A., Cutler, S.R., and Rodriguez, P.L. (2009b). Modulation of drought resistance by the abscisic acid receptor PYL5 through inhibition of clade A PP2Cs. Plant J. *60*, 575–588.

Schroeder, J.I., and Nambara, E. (2006). A quick release mechanism for abscisic acid. Cell *126*, 1023–1025.

Stein, N. (2008). CHAINSAW: a program for mutating pdb files used as templates in molecular replacement. J. Appl. Cryst. *41*, 641–643.

van Loon, L.C., Rep, M., and Pieterse, C.M. (2006). Significance of inducible defense-related proteins in infected plants. Annu. Rev. Phytopathol. *44*, 135–162.

Yin, P., Fan, H., Hao, Q., Yuan, X., Wu, D., Pang, Y., Yan, C., Li, W., Wang, J., and Yan, N. (2009). Structural insights into the mechanism of abscisic acid signaling by PYL proteins. Nat. Struct. Mol. Biol. *16*, 1230–1236.

Yuan, X.Q., Yin, P., Hao, Q., Yan, C.Y., Wang, J.W., and Yan, N.E. (2010). Single amino acid alteration between valine and isoleucine determines the distinct pyrabactin selectivity by PYL1 and PYL2. J. Biol. Chem. *285*, 28953–28958.

Zhu, J.K. (2002). Salt and drought stress signal transduction in plants. Annu. Rev. Plant Biol. *53*, 247–273.